

Supplementary Information to

A structural study of $0.06\text{LiNbO}_3\text{-}0.94\text{K}_{0.5}\text{Na}_{0.5}\text{NbO}_3$ from neutron total scattering analysis

J. Kong,¹ J. Liu,² F. Marlton,³ M. R. V. Jørgensen,^{4,5} A. Pramanick¹

¹Department of Materials Science and Engineering, City University of Hong Kong, Hong Kong, China

²Neutrons Scattering Division, Oak Ridge National Laboratory, Oak Ridge, TN, USA

³Department of Chemistry, University of Sydney, Sydney, NSW, Australia

⁴Department of Chemistry and iNANO, Aarhus University, 8000 Aarhus C, Denmark

⁵MAX IV Laboratory, Lund University, SE-221 00 Lund, Sweden

A. Details of Rietveld refinement of the neutron diffraction patterns

Since our earlier study shows that the monoclinic Pm space group is more adequate to describe unmodified KNN ceramics [S1–S3], we adopted a single-phase Pm space group in the Rietveld refinement against the neutron diffraction patterns of KNNL6 at 290 K, as shown in Fig.S1(a). However, a two-phase $Pm+P4mm$ model yielded a lower R_w of $\sim 4.04\%$ (Fig. 2 (f)) compared to a single-phase model. More importantly, a two-phase model better reproduces the splitting peaks as shown in Fig. 1, such as (311) and (420) shown in Fig. S1(b-c). Therefore, the structure of KNNL6 at 290 K is more likely to be a two-phase coexistence “ $Pm+P4mm$ ” space group.

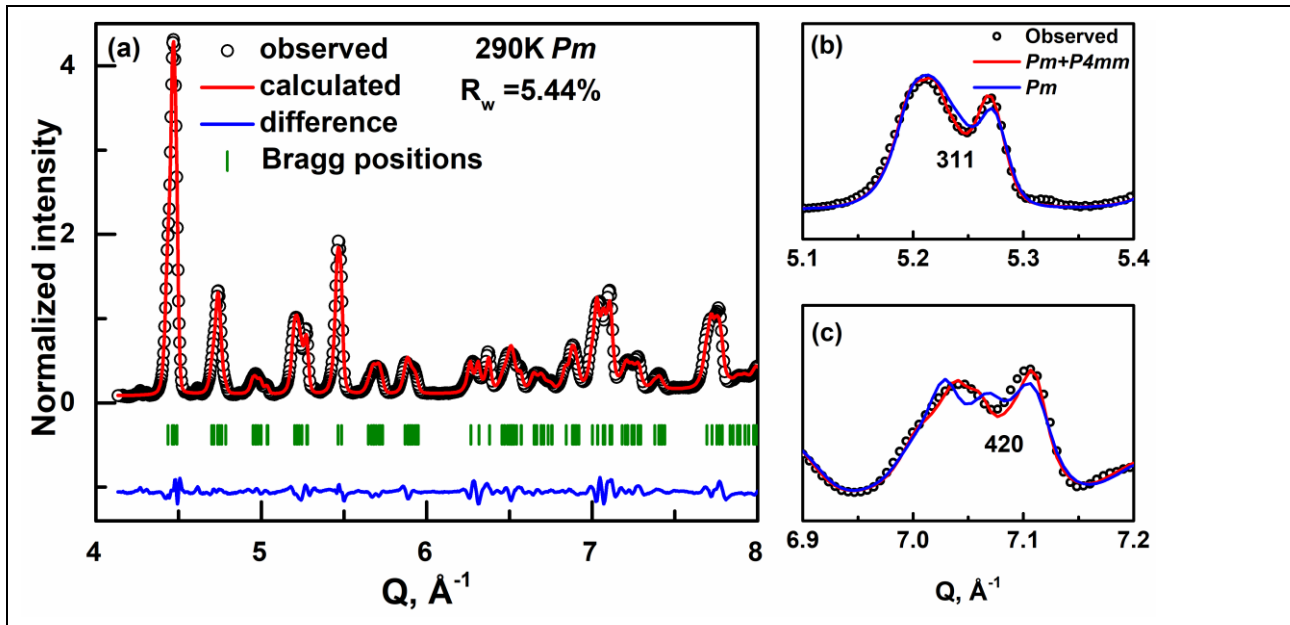


Figure S1. (a) Observed (black symbol), calculated (red line) and difference (blue line) profiles of neutron diffraction patterns of KNNL6 measured at BANK5 of NOMAD, together with the Bragg positions (green ticks). Refinement using single-phase Pm model at 290 K. (b-c) Comparison of experimental (black symbol) and calculated peak profiles for single-phase Pm model (blue line) and two-phase $Pm+P4mm$ model (red line).

We adopted a single-phase Pm space group in the Rietveld refinement against neutron diffraction patterns of KNNL6 at 373 K, as shown in Fig.S2(a). However, a two-phase $Pm+P4mm$ model yielded a lower R_w of $\sim 4.04\%$ (Fig. 2 (e)) compared with a single-phase model. More importantly, a two-phase model better reproduces the splitting peaks as shown in Fig. 1, such as (311) and (420) shown in Fig. S2(b-c). Therefore, the structure of KNNL6 at 373 K is better described by a two-phase coexistence “ $Pm+P4mm$ ” model.

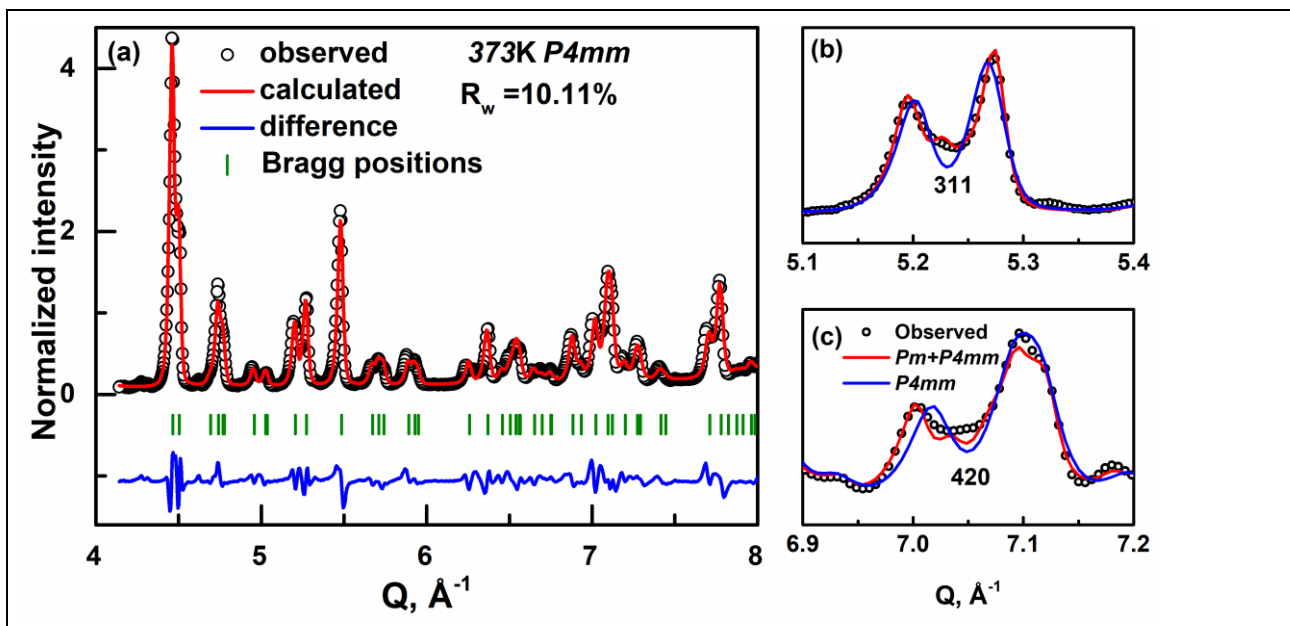


Figure S2. (a) Observed (black symbol), calculated (red line) and difference (blue line) profiles of neutron diffraction patterns of KNNL6 measured at BANK5 of NOMAD, together with the Bragg positions (green ticks). Refinement using single-phase Pm model at 373 K. (b-c) Comparison of experimental (black symbol) and calculated peak profiles for single-phase $P4mm$ model (blue line) and two-phase $Pm+P4mm$ model (red line).

Fig. S3 shows experimental, calculated and difference profiles of neutron diffraction patterns of KNNL6 measured at BANK2 of NOMAD.

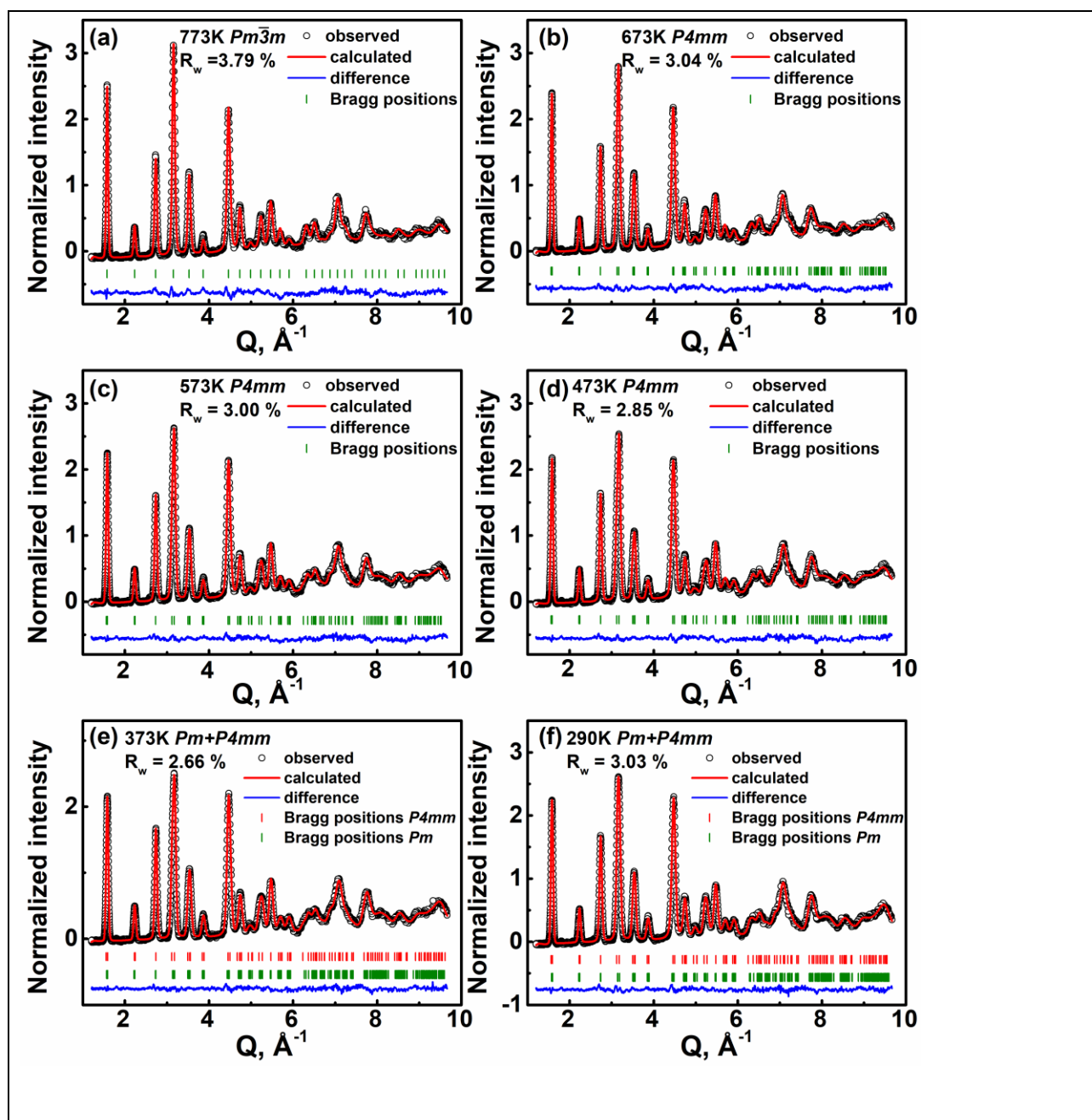


Figure S3. Observed (black symbol), calculated (red line) and difference (blue line) profiles of neutron diffraction patterns of KNNL6 measured at BANK2 of NOMAD, together with the Bragg positions (green ticks). (a) Refinement using $Pm\bar{3}m$ at 773 K; (b) Refinement using $P4mm$ at 673 K; (c) Refinement using $P4mm$ at 573K; (d) Refinement using $P4mm$ at 473 K; (e) Refinement using Pm and $P4mm$ coexistence at 373 K; (f) Refinement using Pm and $P4mm$ coexistence at 290 K.

Fig. S4 shows experimental, calculated and difference profiles of neutron diffraction patterns of KNNL6 measured at BANK3 of NOMAD.

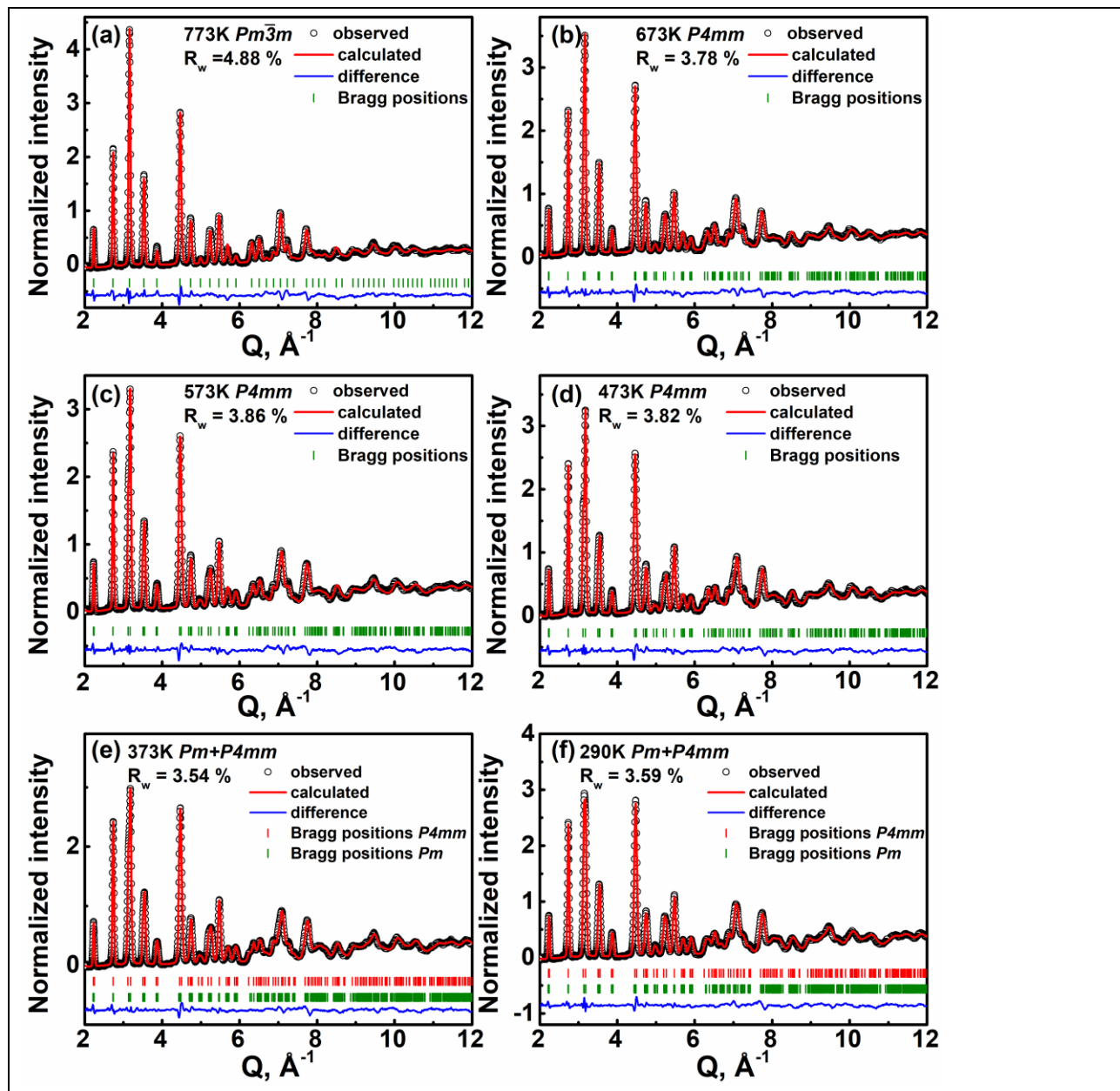


Figure S4. Observed (black symbol), calculated (red line) and difference (blue line) profiles of neutron diffraction patterns of KNNL6 measured at BANK3 of NOMAD, together with the Bragg positions (green ticks). (a) Refinement using $Pm\bar{3}m$ at 773 K; (b) Refinement using $P4mm$ at 673 K; (c) Refinement using $P4mm$ at 573K; (d) Refinement using $P4mm$ at 473 K; (e) Refinement using Pm and $P4mm$ coexistence at 373 K; (f) Refinement using Pm and $P4mm$ coexistence at 290 K.

Fig. S5 shows experimental, calculated and difference profiles of neutron diffraction patterns of KNNL6 measured at BANK4 of NOMAD.

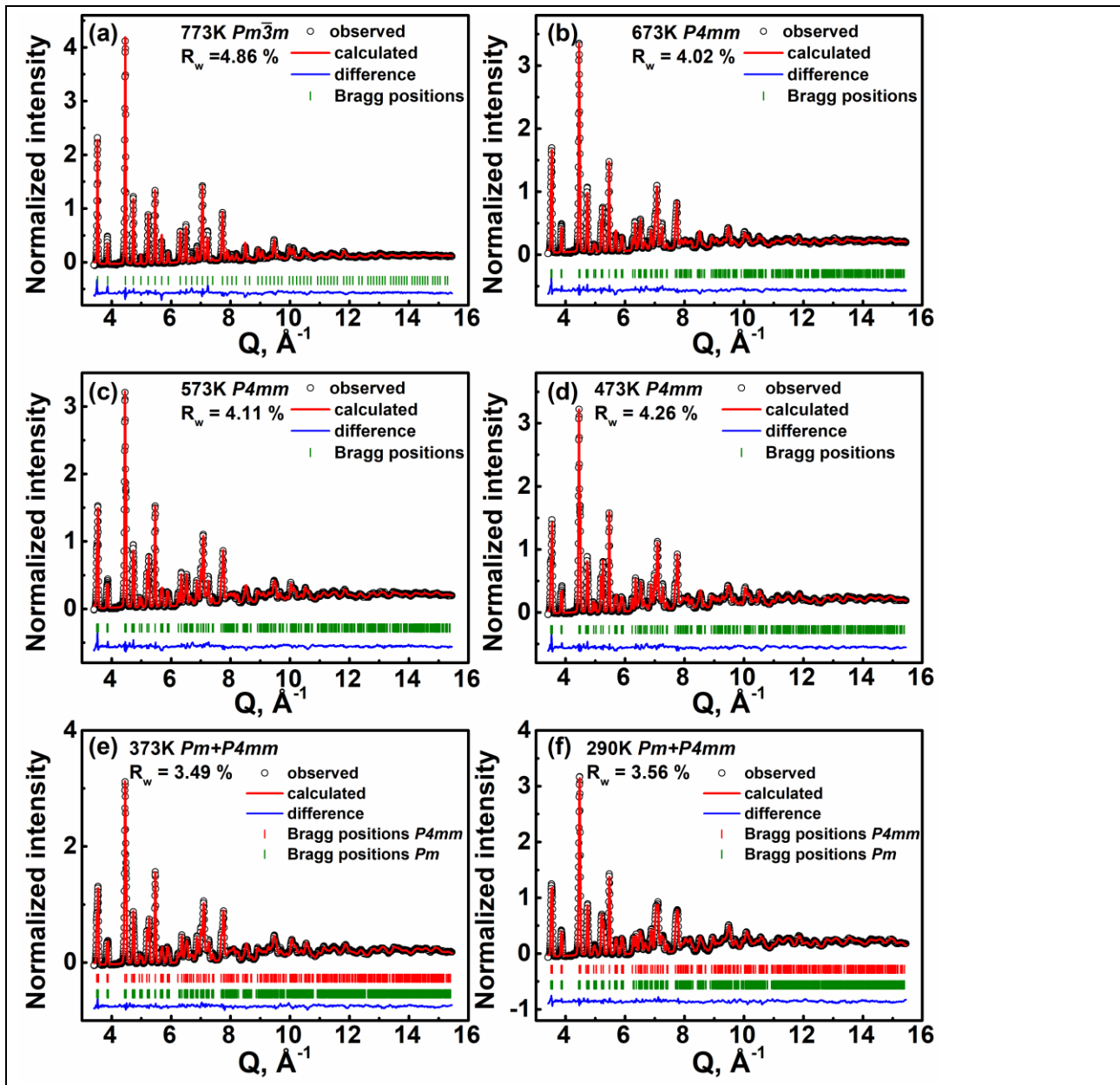


Figure S5. Observed (black symbol), calculated (red line) and difference (blue line) profiles of neutron diffraction patterns of KNNL6 measured at BANK4 of NOMAD, together with the Bragg positions (green ticks). (a) Refinement using $Pm\bar{3}m$ at 773 K; (b) Refinement using $P4mm$ at 673 K; (c) Refinement using $P4mm$ at 573K; (d) Refinement using $P4mm$ at 473 K; (e) Refinement using Pm and $P4mm$ coexistence at 373 K; (f) Refinement using Pm and $P4mm$ coexistence at 290 K.

B. Details of refinement of neutron PDF

Fig. S6(a) shows the experimental and fitted $G(r)$ profiles of the neutron PDF of KNNL6 at 290 K for $r \sim 1.7-10 \text{ \AA}$. Refinement using the $P4mm$ space group got a worse R_w of $\sim 12.06\%$. Therefore, the $P4mm$ structure model cannot reproduce well the peaks at $r \sim 2$ and 2.8 \AA , as shown in Fig. S6 (b). Instead, a Pm model could better describe these peaks as shown in Fig. S6 (b) and Fig.5(a).

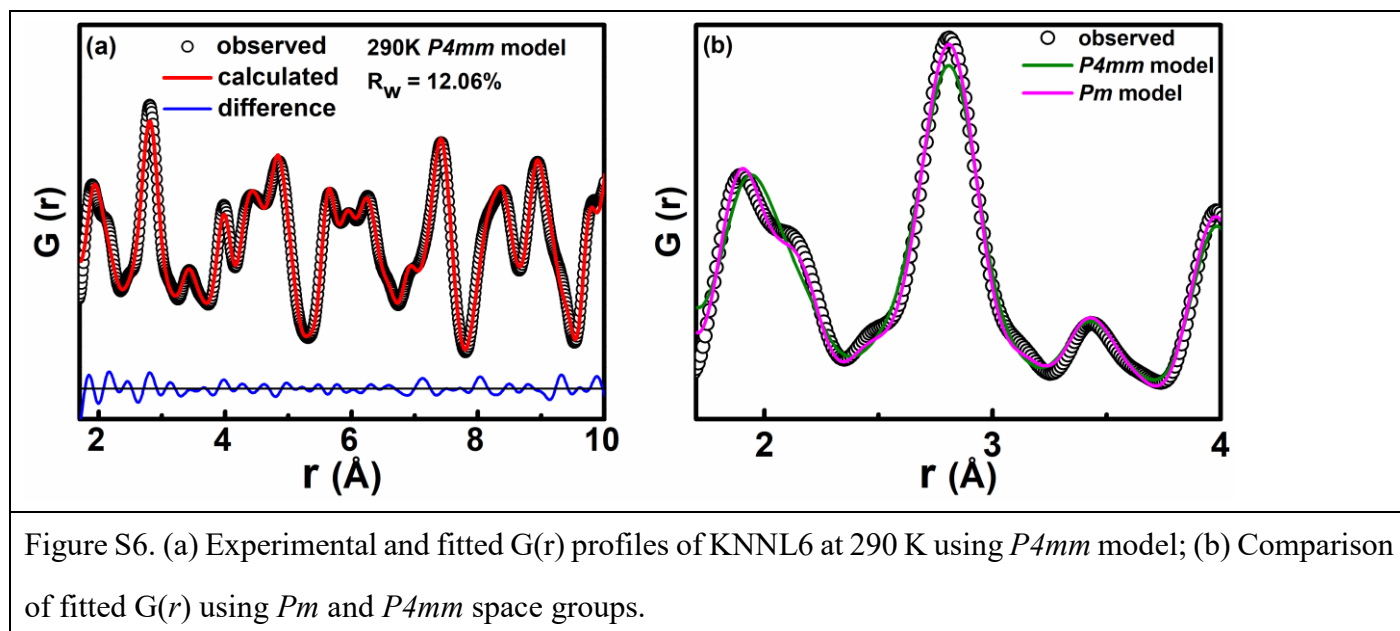


Fig. S7(a) shows the experimental and fitted $G(r)$ profiles of the neutron PDF of KNNL6 at 373 K for $r \sim 1.7-10 \text{ \AA}$. Refinement using the $P4mm$ space group got a worse R_w of $\sim 11.54\%$. Therefore, the $P4mm$ structure model cannot reproduce well the peaks at $r \sim 2$ and 2.8 \AA , as shown in Fig. S7 (b). Instead, a Pm model could better describe these peaks as shown in Fig. S7 (b) and Fig.5(b).

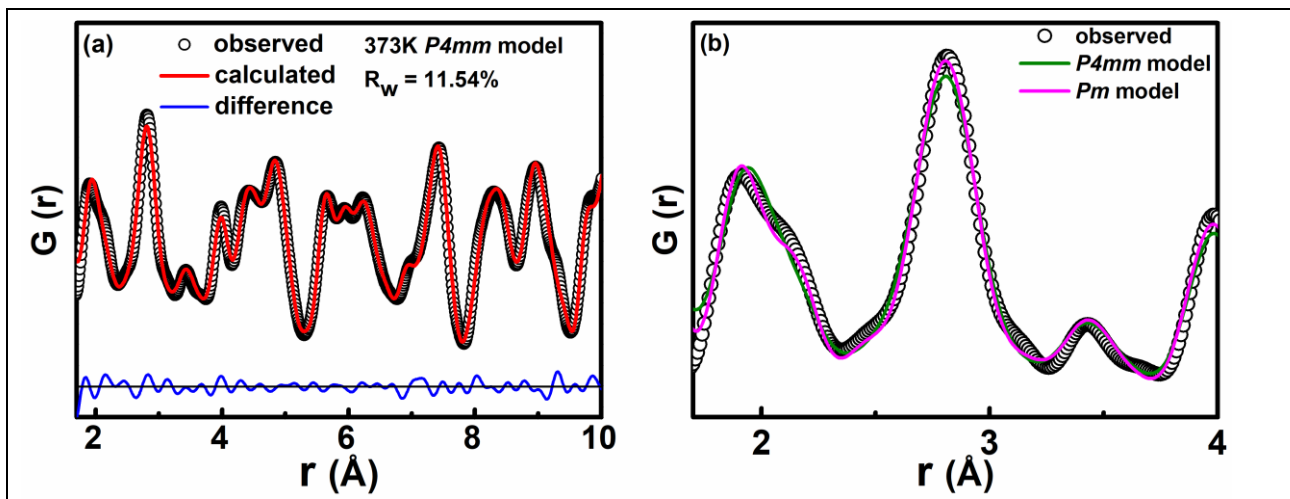


Figure S7. (a) Experimental and fitted $G(r)$ profiles of KNNL6 at 373 K using $P4mm$ model; (b) Comparison of fitted $G(r)$ using Pm and $P4mm$ space groups.

Fig. S8(a) shows the experimental and fitted $G(r)$ profiles of the neutron PDF of KNNL6 at 473 K for $r \sim 1.7-10 \text{ \AA}$. Refinement using the $P4mm$ space group got a worse R_w of $\sim 10.35\%$. Therefore, the $P4mm$ structure model cannot reproduce well the peaks at $r \sim 2$ and 2.8 \AA , as shown in Fig. S8 (b). Instead, a Pm model could better describe these peaks as shown in Fig. S8 (b) and Fig.5(c).

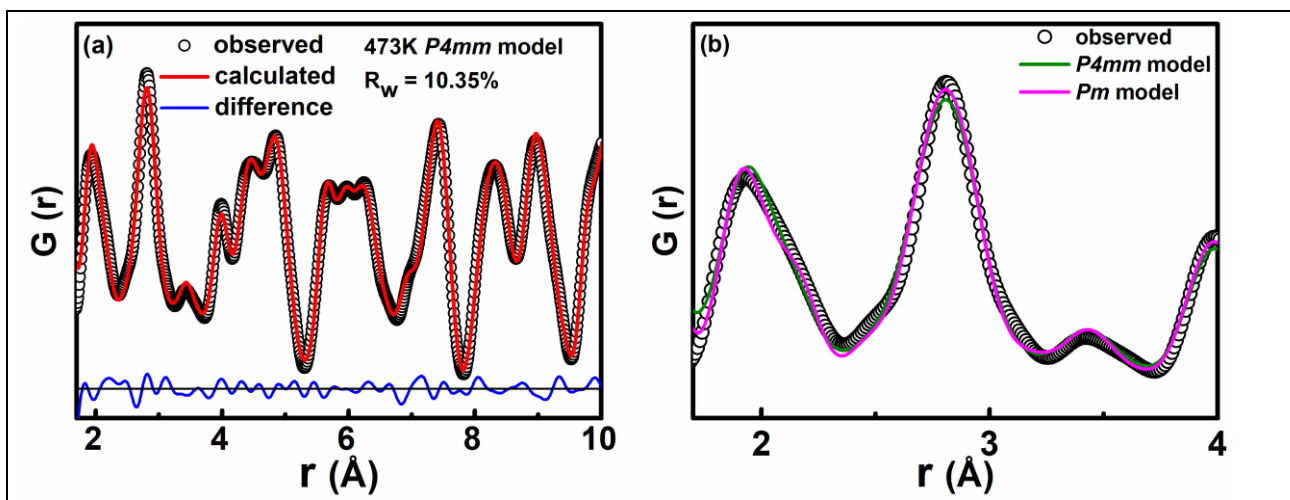


Figure S8. (a) Experimental and fitted $G(r)$ profiles of KNNL6 at 473 K using $P4mm$ model; (b) Comparison of fitted $G(r)$ using Pm and $P4mm$ space groups.

Fig. S9(a) shows the experimental and fitted $G(r)$ profiles of the neutron PDF of KNNL6 at 573 K for $r \sim 1.7-10 \text{ \AA}$. Refinement using the $P4mm$ space group got a worse R_w of $\sim 11.57\%$. Therefore, the $P4mm$ structure model cannot reproduce well the peaks at $r \sim 2$ and 2.8 \AA , as shown in Fig. S9(b). Instead, a Pm model could better describe these peaks as shown in Fig. S9 (b) and Fig.5(d).

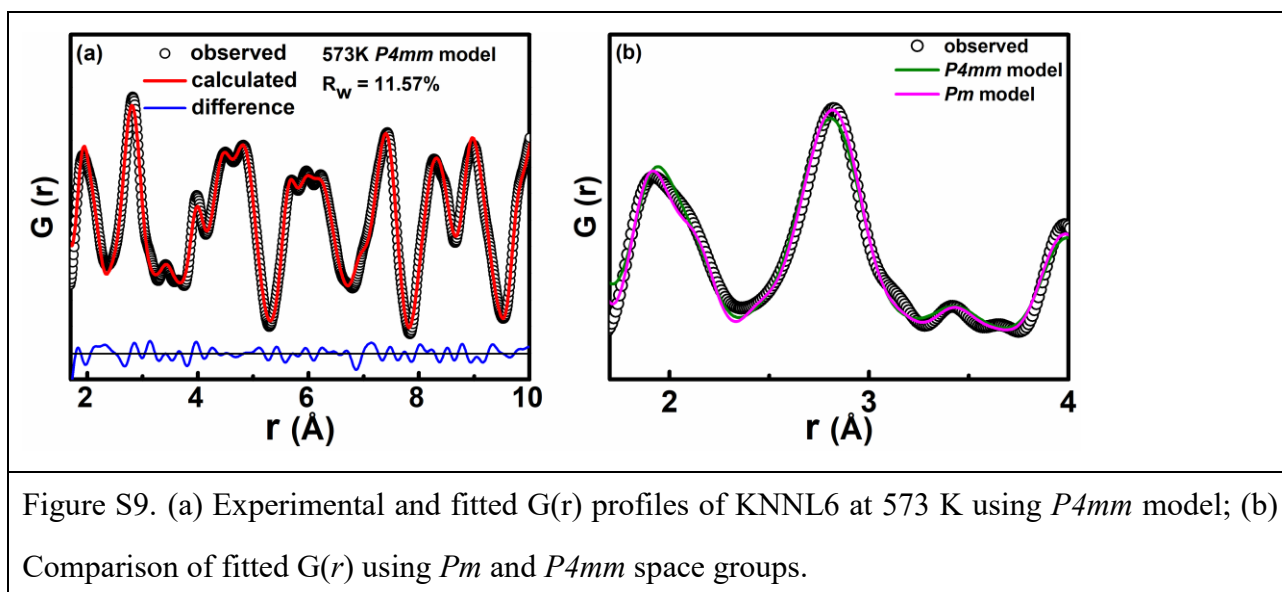


Fig. S10(a) shows the experimental and fitted $G(r)$ profiles of the neutron PDF of KNNL6 at 673 K for $r \sim 1.7-10 \text{ \AA}$. Refinement using the $P4mm$ space group got a worse R_w of $\sim 11.64\%$. Therefore, the $P4mm$ structure model cannot reproduce well the peaks at $r \sim 2$ and 2.8 \AA , as shown in Fig. S10(b). Instead, a Pm model could better describe these peaks as shown in Fig. S10 (b) and Fig.5(e).

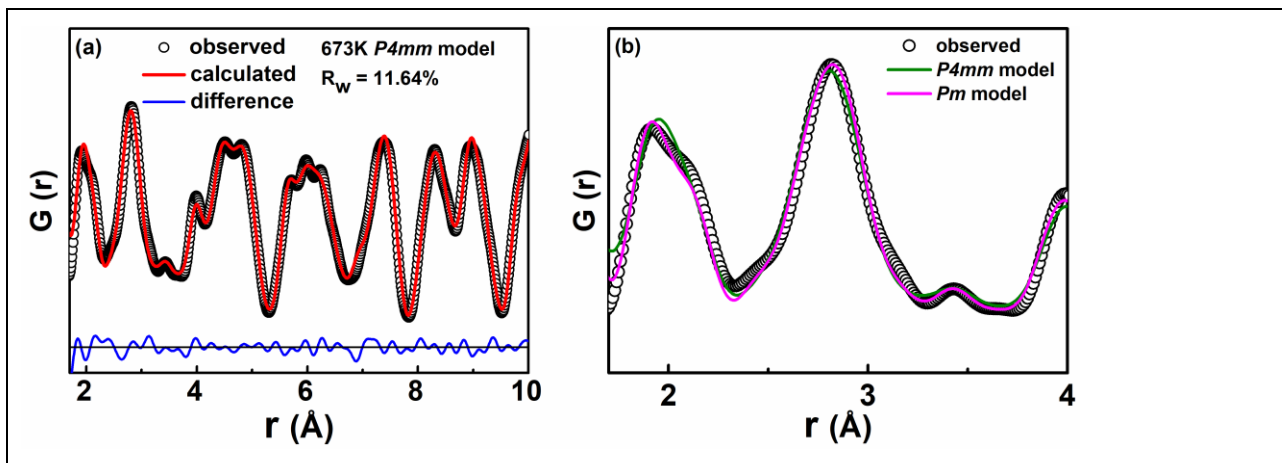


Figure S10. (a) Experimental and fitted $G(r)$ profiles of KNNL6 at 673 K using $P4mm$ model; (b) Comparison of fitted $G(r)$ using Pm and $P4mm$ space groups.

Figs. S11(a-b) shows the experimental and fitted $G(r)$ profiles of the neutron PDF of KNNL6 at 773 K for $r \sim 1.7-10 \text{ \AA}$ using different structure models. Refinement using the $Pm\bar{3}m$ space group yielded an R_w of $\sim 13.60\%$, as shown in Figure S11(a). Refinement using the $P4mm$ space group yielded an R_w of $\sim 12.13\%$, as shown in Figure S11(b). However, both space groups ($Pm\bar{3}m$ and $P4mm$) cannot well reproduce the peak $\sim 4 \text{ \AA}$ compared with the Pm space group shown in Fig. S11(c) and Fig.5(f).

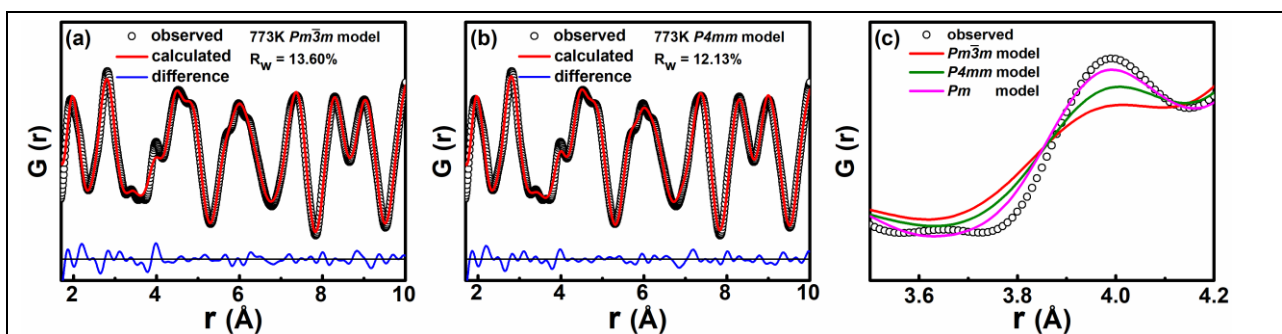


Figure S11. (a) Experimental and fitted $G(r)$ profiles of KNNL6 at 773 K using $Pm\bar{3}m$ model; (b) Experimental and fitted $G(r)$ profiles of KNNL6 at 773 K using $P4mm$ model; (c) Comparison of fitted $G(r)$ using $Pm\bar{3}m$, $P4mm$, and Pm space groups.

Fig. S12(a) shows the structural model of KNNL6, where the K/Na/Li atom occupies the unit cell corners, Nb is near the center of the unit cell, and oxygens are near the face centers. Fig.S12(b) illustrates the displacement of the Nb atom in the monoclinic structure, where the coordinates of Nb are given by $(x, 0.5, z)$. Since the angle β is very close to 90° , fractional displacement of Nb, S , from the high symmetry position $(0.5, 0.5, 0.5)$ can be calculated according to [S4]:

$$S_{\bar{1}00}=x-0.5 \quad (1)$$

$$S_{001}=z-0.5 \quad (2)$$

$$S_{\bar{1}01}=\sqrt{(x-0.5)^2 + (z-0.5)^2} \quad (3)$$

where $S_{\bar{1}00}$ is the displacement along $[\bar{1}00]$ direction, S_{001} is the displacement along $[001]$ direction, $S_{\bar{1}01}$ is the net displacement along $[\bar{1}01]$ direction.

The fractional displacement of the Nb atom in the tetragonal $P4mm$ space group is along $[001]$ since the coordinate of Nb is $(0.5, 0.5, z)$ as shown in Fig.S12(c). Therefore, the fractional displacement can be calculated by equation (2):

$$S_{001}= z-0.5.$$

where S_{001} is displacement along $[001]$ direction.

Nb in the cubic $Pm\bar{3}m$ structure is at the center of the unit cell. Therefore, the fractional displacement is 0 since the coordinates of Nb is $(0.5, 0.5, 0.5)$.

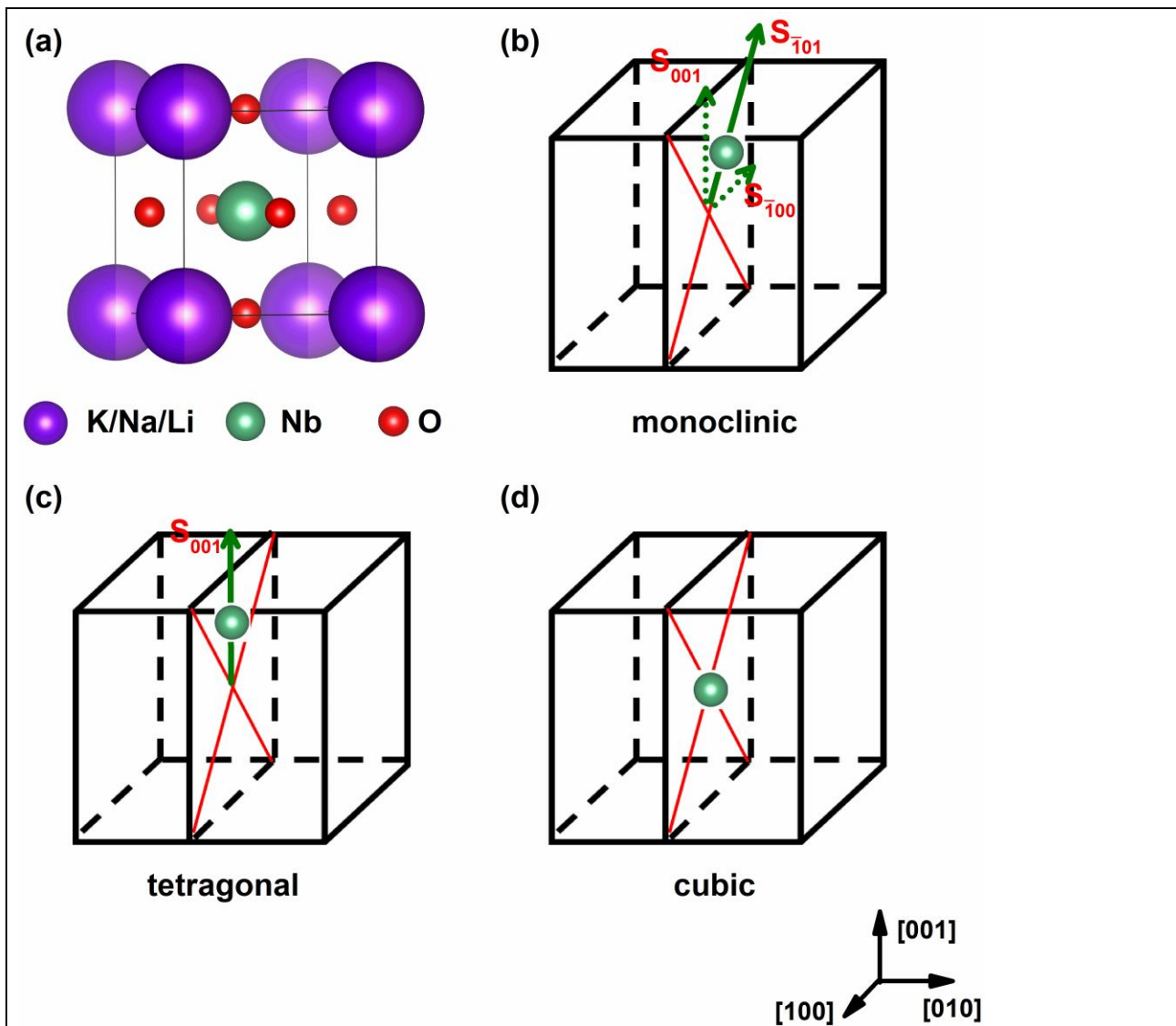


Figure S12. (a) Structure model of KNNL6, where the K/Na/Li atom occupies the unit cell corners, Nb is near the center of the unit cell, and oxygens are near the face centers. (b) Description of Nb displacement in the monoclinic phase with coordinates $(x, 0.5, z)$. (c) Description of Nb displacement in the tetragonal phase with coordinates $(0.5, 0.5, z)$. (d) Description of Nb displacement in the cubic phase with coordinates $(0.5, 0.5, 0.5)$.

Figs.S13(a-b) are the neutron PDF $G(r)$ for $r \sim 1.6-2.4 \text{ \AA}$, which indicate the nearest neighbor Nb-O bond distances. Fitting of the low-temperature 290 K and high-temperature 773 K patterns using two Gaussian functions are shown, respectively. It is apparent that the peak for Nb-O nearest neighbor bond distances bond peak is split at both low and high temperatures, although the two subpeaks are broader at 773 K due to increased thermal vibrations.

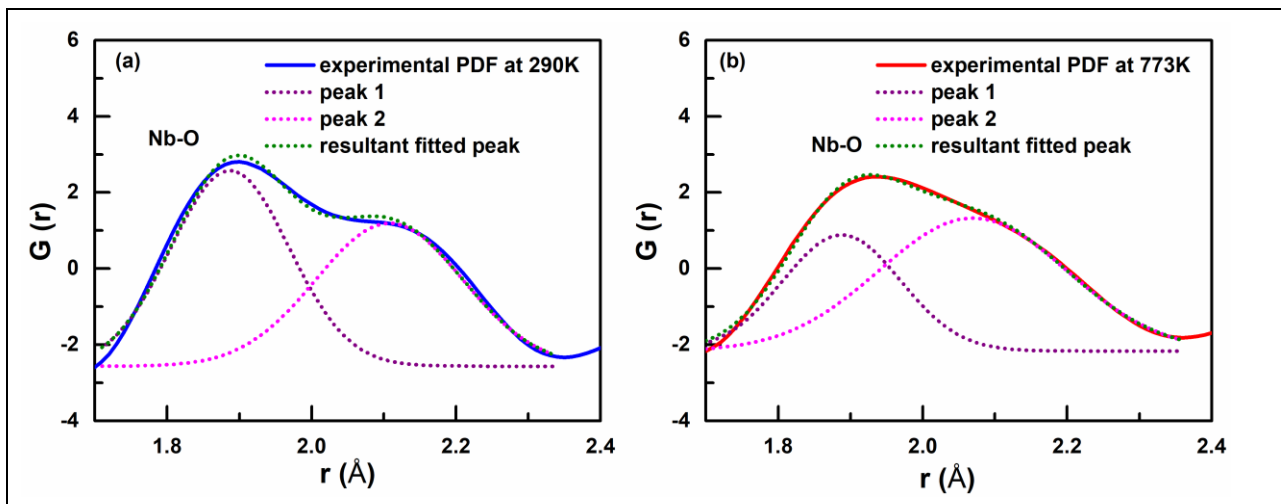


Figure S13. $G(r)$ for Nb-O bond peaks fitted with Gaussian Function: (a) $G(r)$ at 290 K; (b) $G(r)$ at 773 K.

C. Introduction for NOMAD at the SNS

The Nanoscale Ordered Materials Diffractometer (NOMAD) is a neutron time-of-flight diffractometer designed to determine pair distribution functions of a wide range of materials ranging from short range ordered liquids to long range ordered crystals.[S5] The detailed information, including experimental setup, instrument characteristic, and so on could be seen in Ref [S6-S7].

References

- S1. Baker, D.W.; Thomas, P.A.; Zhang, N.; Glazer, A.M. A comprehensive study of the phase diagram of $K_xNa_{1-x}NbO_3$. *Appl. Phys. Lett.* **2009**, *95*, 91903, doi:10.1063/1.3212861.
- S2. Baker, D.W.; Thomas, P.A.; Zhang, N.; Glazer, A.M. Structural study of $K(x)Na(1-x)NbO(3)$ (KNN) for compositions in the range $x = 0.24-0.36$. *Acta Crystallogr. B* **2009**, *65*, 22–28, doi:10.1107/S0108768108037361.
- S3. Gupta, S.; Petkov, V.; Priya, S. Local atomic structure of $K_xNa(1-x)NbO_3$ by total x-ray diffraction. *Appl. Phys. Lett.* **2014**, *105*, 232902, doi:10.1063/1.4903512.
- S4. Veselinović, L.; Mitrić, M.; Avdeev, M.; Marković, S.; Uskoković, D. New insights into $BaTi_{1-x}Sn_xO_3$ ($0 \leq x \leq 0.20$) phase diagram from neutron diffraction data. *J Appl Crystallogr* **2016**, *49*, 1726–1733, doi:10.1107/S1600576716013157.
- S5. Neuefeind, J.; Feygenson, M.; Carruth, J.; Hoffmann, R.; Chipley, K.K. The Nanoscale Ordered Materials Diffractometer NOMAD at the Spallation Neutron Source SNS. *Nuclear Instruments and Methods in Physics Research Section B: Beam Interactions with Materials and Atoms* **2012**, *287*, 68–75, doi:10.1016/j.nimb.2012.05.037.
- S6. Usher, T.-M.; Forrester, J.S.; McDonnell, M.; Neuefeind, J.; Page, K.; Peterson, P.F.; Levin, I.; Jones, J.L. Time-of-flight neutron total scattering with applied electric fields: Ex situ and in situ studies of ferroelectric materials. *Rev. Sci. Instrum.* **2018**, *89*, 92905, doi:10.1063/1.5037609.
- S7. Calder, S.; An, K.; Boehler, R.; Dela Cruz, C.R.; Frontzek, M.D.; Guthrie, M.; Haberl, B.; Huq, A.; Kimber, S.A.J.; Liu, J.; et al. A suite-level review of the neutron powder diffraction instruments at Oak Ridge National Laboratory. *Rev. Sci. Instrum.* **2018**, *89*, 92701, doi:10.1063/1.5033906.